amplifiers limited to 85-v output; 4) cause no change in precession constant or side balance of the accelerometer; and 5) contribute no residual or constant torque.

A torquing unit using a polarized solenoid was tried first. It met most of the requirements and proved the feasibility of the concept, but it had residual torques that required cancellation through electrical biasing. The design subsequently adopted (Fig. 2) met all of the requirements and eliminated the biasing problem. An important feature is the extended active length of the coil. The torquer unit was designed to use all of the available space on the mass balance end of the air bearing cylinder. The four-coil, four-magnet-cup unit provides the symmetry necessary to keep the inner cylinder balanced. The arrangement in two pairs of back-to-back magnet cups enhances the keeper quality of the steel cups and provides for very accurate calibration, because the number of active turns remains constant as the magnets move into and away from the coil bobbins during the small rotational movements of the inner cylinder; the magnets move toward two of the layer-wound coils as they move away from the remaining two. Polarized magnets allow all of the coils to be active during either positive or negative rotation of the accelerometer measuring head.

The precession (output) of an integrating accelerometer results from a torque T on its input axis which follows the gyro law $T = \omega H$. The simulated torque per g of acceleration (T/g, g-cm) is provided by the force and moment arm of the magnet-coil assembly as follows:

$$T/g = \omega H/g = fl = (10^{-7}\,\beta LI/g)l \qquad (1)$$

where g = gravitational acceleration, 980 cm/sec^2; ω = precession rate, rad/sec; H = angular momentum of wheel g-cm^2/sec; f = force, g; l = moment arm, cm; the constant 10^{-7} results from the units chosen for β, L, and I; β = flux density, gauss; L = active wire length, cm; and I = current, ma.

For this particular accelerometer, $H = 1.15 \times 10^5$ g-cm^2/sec, and a 1-g input causes precession at 0.210 rad/sec, so that $T/g = 24.6$ g-cm, or 6.15 g-cm for each of the four magnet cups. The size of the nylon coil bobbin and the coil wire were governed by available space and slip-ring current limitations. The design chosen uses 324 active turns of number 42 wire on a mean coil diameter of 0.762 cm, giving L = 775 cm/coil. The moment arm l is 1.6 cm. If it is assumed that $\beta = 800$ gauss, then by Eq. (1) $I = 6.15g/10^{-7}\,(800)(775)(1.6) = 61$ ma. In practice, more current than this was required, hence the flux density was somewhat less than 800 gauss for the magnet material used.

The four magnets are charged to saturation as an assembly and are subject to the sustained keeper action of the steel cups. The stray magnetic field problem, although greatly reduced by the magnet-cup configuration, still must be considered. All parts of the coil assembly must be entirely nonmagnetic. (One of the original wiring terminals appeared to be tinned copper but had a very slight magnetic property, which was not detected until the unit demonstrated a residual torque during preliminary testing.)

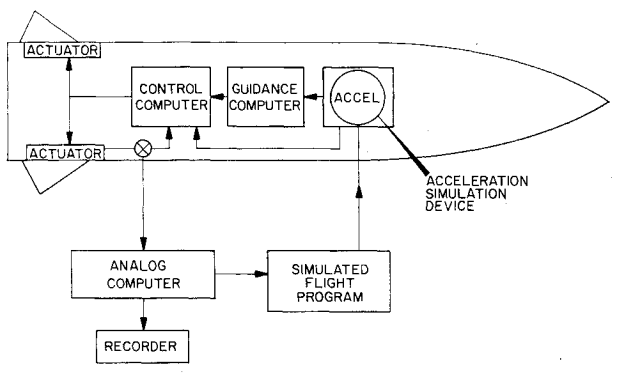

Fig. 1. Loop completion.

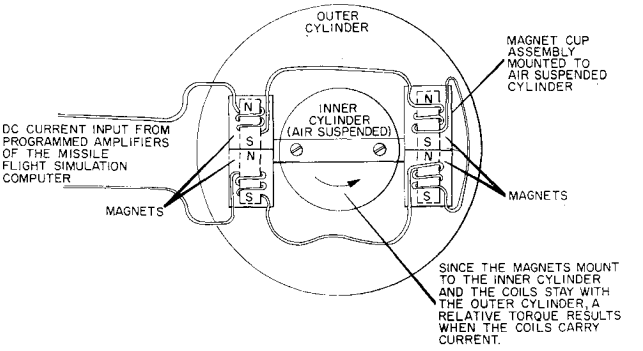

Fig. 2. Torquer configuration.

Calibration

For accelerations up to 1g, calibration of the torquer was accomplished by coupling accurate fractional components of the local gravity vector into the sensitive axis of the accelerometer and applying current to the torquer to cancel the resulting precession rate. For accelerations from 1 to 3g, the torquer was used to drive out the existing 1-g value and to generate an opposite precession rate equal to various g increments. All of this calibration was accomplished with the readout instrumentation already available for the accelerometer.

Stability of Constant-Altitude Re-Entry Flight Paths

ALLEN R. STUBBERUD*
University of California, Los Angeles, Calif.

ONE method of guidance of lifting bodies entering the earth's atmosphere at superorbital velocities is flight-path control, that is, the controlling of the body to fly a prechosen nominal flight path or trajectory.[1] A total re-entry trajectory is generally obtained by piecing together several simple trajectories such as constant-altitude or equilibrium-glide trajectories.[2] A question of concern in the method of flight-path control is that of the stability of the trajectory, that is, the property of the trajectory which determines whether or not the lifting body returns to the nominal trajectory without the application of control command whenever it is perturbed from the trajectory. In this note the stability of the class of constant-altitude trajectories is examined.

Velocity as the Independent Variable

The motion of the center of gravity of a lifting body entering the earth's atmosphere under the assumptions that 1) the earth is spherical and nonrotating; 2) the atmospheric density is exponential ($\rho = \rho_0 e^{-\beta h}$); and 3) the motion of the body is planar, is described by the set of equations

$$V\dot{\gamma} = -L/m - (V^2/r)\cos\gamma + g\cos\gamma \qquad (1)$$

$$\dot{V} = -D/m + g\sin\gamma \qquad (2)$$

$$\dot{\rho} = \beta V\rho\sin\gamma \qquad (3)$$

Received October 16, 1964; revision received March 19, 1965.
* Assistant Professor, Department of Engineering.

where V, L, and D are the magnitudes of the velocity, lift, and drag vectors, respectively; γ is the angle between local horizontal and velocity vector, measured positive downward; m is the mass of the body; r is the distance from earth's center to the body; g is the gravitational constant; h is the altitude of vehicle above the earth's surface; ρ and ρ_0 are the atmospheric densities at altitude h and at sea level, respectively; and β is the exponential decay constant of the atmosphere.

Several of the classes of trajectories which have been proposed for lifting re-entry are most appropriately described in the h-V plane, that is, the altitude is defined as a function of velocity and vice versa.[2] Following this precedent, time as the independent variable is eliminated among Eqs. (1–3), and V is used as the independent variable in the remaining two equations. An important question is whether the new independent variable V is monotonic with time. Examination of Eq. (2) shows that V decreases monotonically if

$$D/m > g \sin\gamma \tag{4}$$

Since D/m can be written

$$D/m = \rho V^2 g(C_D A/W)/2 \tag{5}$$

inequality (4) can be rewritten

$$V^2 > (W/C_D A)(2/\rho) \sin\gamma \tag{6}$$

where W is the vehicle's weight, C_D is its drag coefficient ($C_D = 2D/\rho V^2 A$), and A is its reference cross-sectional area; $W/C_D A$ is its ballistic coefficient. A typical set of re-entry conditions are: $V = 35{,}000$ fps, $\gamma = 0.1$ rad, and $h = 300{,}000$ ft ($\rho = (1.05)10^{-8}$ slug/ft^3). In this case $W/C_D A < 645$ guarantees the monotonicity of V. This value probably includes most re-entry vehicles. In addition, as altitude decreases (ρ increases), the drag increases rapidly enough to assure inequality (4).

It is more convenient to use as the independent variable the normalized velocity $\mathbf{V} = V/V_s$ that has the same monotonic property as V. The normalizing velocity $V_s = (rg)^{1/2}$ (orbital velocity) will be assumed a constant over the values of r and g of interest. Now differential equations for γ and ρ can be written as

$$\frac{d\gamma}{d\mathbf{V}} = \frac{d\gamma}{dt}\left(\frac{1}{\dot{\mathbf{V}}}\right) = \frac{-L + mg(1 - \mathbf{V}^2)\cos\gamma}{[-D + mg\sin\gamma]\mathbf{V}} \tag{7}$$

$$\frac{d\rho}{d\mathbf{V}} = \frac{d\rho}{dt}\left(\frac{1}{\dot{\mathbf{V}}}\right) = \frac{mV_s^2\mathbf{V}^2\beta\rho\sin\gamma}{[-D + mg\sin\gamma]\mathbf{V}} \tag{8}$$

where

$$L = \tfrac{1}{2}\rho\mathbf{V}^2 V_s^2 C_L A \tag{9}$$

$$D = \tfrac{1}{2}\rho\mathbf{V}^2 V_s^2 C_D A \tag{10}$$

Linearized Equations About a Constant-Altitude Flight Path

For constant-altitude flight, $\gamma = 0$, $L = mg(1 - \mathbf{V}^2)$, and ρ is a constant, say ρ_d. Now a pair of linear differential equations which describe the motion about a constant-altitude flight path can be formed by sustituting the following in Eqs. (7) and (8): $\rho = \rho_d + \delta\rho$, $\gamma = \delta\gamma$, $C_D = C_{Dn} + \delta C_D$, and $C_L = C_{Ln} + \delta C_L$, where C_{Dn} and C_{Ln} are the nominal values of C_D and C_L associated with the constant-altitude flight path. The pair of linear equations thus formed are:

$$d(\delta\rho)/d\mathbf{V} = -(mV_s^2\mathbf{V}\beta\rho_d/D)\delta\gamma \tag{11}$$

$$d(\delta\gamma)/d\mathbf{V} = (L/D\rho\mathbf{V})\delta\rho + (L/D\mathbf{V})\delta CL/CL_n \tag{12}$$

where L and D are the nominal values of lift and drag. Substituting for D as given in Eq. (10), Eq. (11) can be rewritten

$$d(\delta\rho)/d\mathbf{V} = -(2m\beta/\mathbf{V}C_{Dn}A)\delta\gamma \tag{13}$$

If the component of L in the plane of re-entry is controlled by changing the bank angle and maintaining a constant angle of attack, then C_D is assumed to be constant, and Eqs. (12) and (13) can be combined by 1) differentiating Eq. (13) with respect to V and 2) in the resulting equation substituting the values for $\delta\gamma$ and $d(\delta\gamma)/d\mathbf{V}$ as given by Eqs. (13) and (12), respectively. The resulting second-order equation for $\delta\rho$ is

$$\frac{d^2(\delta\rho)}{d\mathbf{V}^2} + \frac{1}{\mathbf{V}}\frac{d(\delta\rho)}{d\mathbf{V}} + \left[\frac{k^2(1 - \mathbf{V}^2)}{\mathbf{V}^4}\right]\delta\rho = \left[\frac{k^2\rho_d(1 - \mathbf{V}^2)}{\mathbf{V}^4}\right]\frac{\delta C_L}{C_{Ln}} \tag{14}$$

where

$$k^2 = \frac{4m^2\beta g}{\rho_d^2 C_{Dn}^2 A^2 V_s^2} = \frac{4(W/C_D A)^2\beta}{\rho_d^2 g V_s^2}$$

and $\mathbf{V}_0 \geq \mathbf{V} \geq 0$, where $\mathbf{V}_0$ is the normalized re-entry velocity.

Now define a new independent variable $\tau = k/\mathbf{V}$ and rewrite Eq. (14) in terms of τ, that is

$$\frac{d^2\delta\rho}{d\tau^2} + \frac{1}{\tau}\frac{d\delta\rho}{d\tau} + \left(1 - \frac{k^2}{\tau^2}\right)\delta\rho = \rho_d\left(1 - \frac{k^2}{\tau^2}\right)\frac{\delta C_L}{C_{Ln}} \tag{15}$$

where the independent variable τ is defined over the region $\tau_0 = k/\mathbf{V}_0 \leq \tau < +\infty$. Since ρ_d is a constant, the following definitions can be made: $\bar{\rho} = \delta\rho/\rho_d$, and $\bar{C}_L = \delta C_L/C_{Ln}$. Equation (13) can be rewritten

$$\frac{d^2\bar{\rho}}{d\tau^2} + \frac{1}{\tau}\frac{d\bar{\rho}}{d\tau} + \left(1 - \frac{k^2}{\tau^2}\right)\bar{\rho} = \left(1 - \frac{k^2}{\tau^2}\right)\bar{C}_L \tag{16}$$

The stability of the constant-altitude flight path is apparently determined by the homogeneous portion of Eq. (16), that is

$$\frac{d^2\bar{\rho}}{d\tau^2} + \frac{1}{\tau}\frac{d\bar{\rho}}{d\tau} + \left(1 - \frac{k^2}{\tau^2}\right)\bar{\rho} = 0 \tag{17}$$

The solution of this equation can be written[3,4]

$$\bar{\rho}(\tau) = AJ_k(\tau) + BY_k(\tau) \tag{18}$$

where $J_k(\tau)$ is the Bessel function of the first kind of order k, and $Y_k(\tau)$ is the Bessel function of the second kind of order k. A and B are functions of the initial conditions $\bar{\rho}(\tau_0)$ and $(d\bar{\rho}/d\tau)_{\tau=\tau_0}$. It is straightforward to show that the complete solution can be written

$$\bar{\rho}(\tau) = \frac{\Pi\tau_0}{4}\left\{[Y_{k-1}(\tau_0) - Y_{k+1}(\tau_0)]\bar{\rho}(\tau_0) - 2Y_k(\tau_0)\left.\frac{d\bar{\rho}}{d\tau}\right|_{\tau=\tau_0}\right\}J_k(\tau) + \frac{\Pi\tau_0}{4}\left\{2J_k(\tau_0)\left.\frac{d\bar{\rho}}{d\tau}\right|_{\tau=\tau_0} + [J_{k+1}(\tau_0) - J_{k-1}(\tau_0)]\bar{\rho}(\tau_0)\right\}Y_k(\tau) \tag{19}$$

which is the closed-form solution for the percentage variation in air density from the nominal air density ρ_d.

For values of $W/C_D A$ in the order of 100 and nominal altitudes between 150,000 and 250,000 ft, k is in the order of 50, and τ is approximately the same since $\mathbf{V} \cong 1$. Under these conditions $J_k(\tau)$ and $Y_k(\tau)$ can be approximated as follows:[5] for $\tau > k$, i.e., $\mathbf{V} < 1$

$$J_k(\tau) \cong [(2\cot\beta)/\Pi k]^{1/2}\cos[k(\tan\beta - \beta) - \Pi/4] \tag{20}$$

$$Y_k(\tau) \cong [(2\cot\beta)/\Pi k]^{1/2}\sin[k(\tan\beta - \beta) - \Pi/4] \tag{21}$$

where $\cos\beta = k/\tau = \mathbf{V}$. Since $\mathbf{V}$ decreases monotonically with time, then β, $\tan\beta$, and $\tan\beta - \beta$ increase monotonically with time. In this region, $\bar{\rho}(\tau)$ is then oscillatory but with

decreasing amplitude as time increases. For $\tau < k$, i.e., $\mathbf{V} > 1$

$$J_k(\tau) \cong [\tfrac{1}{2}\Pi k \tanh\alpha]^{1/2} \exp[-k(\alpha - \tanh\alpha)] \quad (22)$$

$$Y_k(\tau) \cong [2/\Pi k \tanh\alpha]^{1/2} \exp[k(\alpha - \tanh\alpha)] \quad (23)$$

where $\cosh\alpha = k/\tau = \mathbf{V}$. Since $\mathbf{V}$ decreases monotonically with time, then α, $\tanh\alpha$, $\alpha - \tanh\alpha$ increase monotonically with time.

The general characteristics of $\bar{\rho}(\tau) = \bar{\rho}(k/\mathbf{V})$ can be summarized as follows: 1) for $\mathbf{V} > 1$, $\bar{\rho}$ tends to increase exponentially with decreasing $\mathbf{V}$ as approximated by the form of $Y_k(\tau)$ in Eq. (23); 2) for $\mathbf{V} = 1$, since both $J_k(k)$ and $Y_k(k)$ have finite values for $k \neq 0$, $\bar{\rho}$ attains a finite value; and 3) for $\mathbf{V} < 1$, $\bar{\rho}$ will be oscillatory in nature but with decreasing amplitude. From the nature of the solution in Eq. (19), as $\mathbf{V} \to 0$, $\tau \to \infty$, and $\bar{\rho}(\tau) \to 0$. Thus this equation indicates that the system is stable for small perturbations in air density about the nominal air density.

Analog Simulation of Constant-Altitude Glide

In order to verify the validity of Eq. (17) as an adequate approximation of the equations of the motion of a re-entry body about a constant-altitude trajectory, an analog computer study was made. For this study, Eqs. (1–3) were transformed into a more convenient form for studying the nonlinear perturbations about a given constant-altitude flight path. These transformed equations were simulated on the computer. The transformation was accomplished through the following change of variables:

$$\rho = \rho_d\rho^* \quad (24)$$

$$V = V_s\mathbf{V} = (rg)^{1/2}\mathbf{V} \quad (25)$$

$$L/D = 2(W/C_DA)(1 - V^2)/\rho_dV^2 \quad (26)$$

where Eq. (26) defines the value of L/D which produces zero net vertical acceleration, and the relationship between $\bar{\rho}$ and ρ^* is given as

$$\bar{\rho} = \delta\rho/\rho_d = (\rho - \rho_d)/\rho_d = (\rho_d\rho^* - \rho_d)/\rho_d = \rho^* - 1 \quad (27)$$

Equations (1–3) under these variable changes become

$$(r/g)^{1/2}\dot{\gamma} = (\mathbf{V}^2 - 1)[\rho^*/\mathbf{V} - (\cos\gamma)/\mathbf{V}] \quad (28)$$

$$(r/g)^{1/2}\dot{\mathbf{V}} = -[\rho_d\dot{V}_s^2/2(W/C_DA)]\rho^*\mathbf{V}^2 + \sin\gamma \quad (29)$$

$$\dot{\rho}^* = \beta V_s\rho^*\mathbf{V}\sin\gamma \quad (30)$$

To provide constants for the simulation the following parameters were chosen: $W/C_DA = 50$, $\mathbf{V}_0 = 1.25$, $|L/D| \leq 1$, and $\rho_d = (3.32)10^{-7}$ slugs/ft^3 ($h = 211{,}500$ ft). For these parameter values, Eq. (26) becomes

$$L/D = 0.447(1 - \mathbf{V}^2)/\mathbf{V}^2 \quad (31)$$

Since $|L/D| \leq 1$, the computer solution is valid only over the region

$$0.557 \leq \mathbf{V} < +\infty \quad (32)$$

From the simulation of Eqs. (27–30), curves of $\bar{\rho}$ vs $\mathbf{V}$ were obtained on an x-y plotter. During each computer run, $\mathbf{V}$ was monitored and was found in each case to decrease monotonically with time. The results for values of initial perturbations $\bar{\rho}$ in air density of -10% and $\pm 20\%$ of the nominal air density are given in Figs. 1a–1c. On the same values figures of $\bar{\rho}$ are plotted which were calculated by evaluating Eq. (19) for the same initial conditions. Values for the Bessel functions were found in Refs. 4 and 5. The general curve shapes are similar, but the point-by-point amplitudes differ significantly. A significant portion of this difference is probably caused by the fact that the computer produced a significant output even when the initial perturbations were made as nearly zero as possible. Figure 1d illustrates this phenomenon. This result is not surprising in view of the exponential form of the perturbation as approximated by Eqs. (19, 22, and 23). Any noise, which is inevitable in an analog computer, would excite these exponential-like responses. The computer results in Figs. 1a–1d were all run at the same time; therefore, it is not unreasonable to assume that similar disturbances were present in each run. Since the run represented by Fig. 1d has the smallest amplitude, it most closely represents a linear perturbation. Assuming that the disturbances in each of the runs in Figs. 1a–1c were the same, then the differences between the computer results and calculated results should differ approximately by the value of the perturbation in Fig. 1d. A set of "corrected" calculated results was obtained by adding the curve in Fig. 1d to Figs. 1a–1c. Comparison of these corrected results with the computer results in Figs. 1e–1g is seen to be much more favorable.

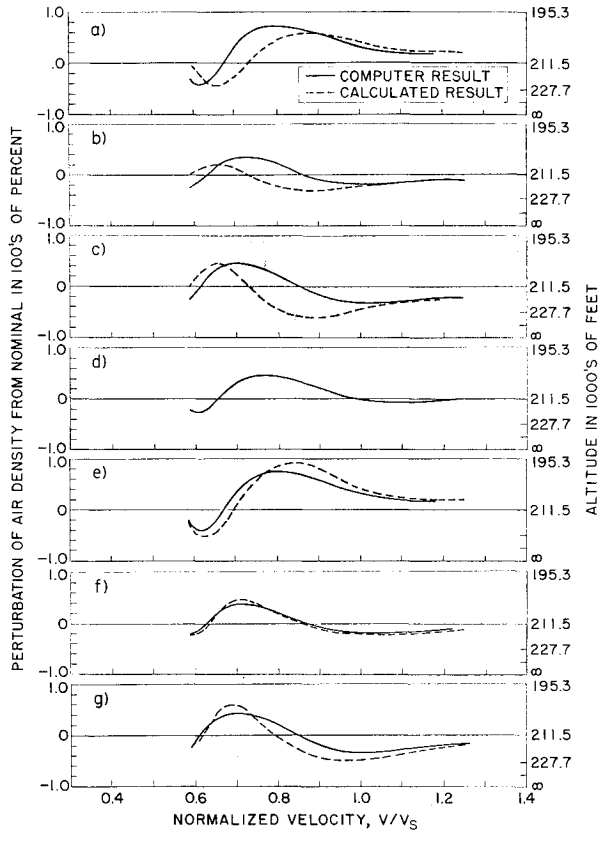

Fig. 1 Air density perturbation vs velocity; initial condition, % of nominal: a) 20, b) − 10, c) − 20, d) 0, e) 20, f) − 10, g) − 20.

Summary

The formulation used for this perturbation analysis of the stability of the class of constant-altitude re-entry flight paths is believed to be different from those used previously. It leads to a Bessel equation that describes perturbation in air density (and consequently altitude) about the nominal constant air density. An analog simulation of the nonlinear re-entry equations was used to obtain "exact" solutions that indicate that the linear perturbations approximate the nonlinear perturbations quite closely and are adequate for at least a qualitative analysis of a constant-altitude trajectory.

One additional comment can be made about the linearized Eq. (16). The equation could be used as a guidance equation for constant-altitude re-entry, that is, the corrective effect $\bar{C}_L$ would be chosen as a function of velocity rather than time as is the case with standard linearized equations.

References

[1] Vaeth, J. R., "Re-entry guidance and flight path control," Inst. Radio Engrs. Trans. Space Electron. Telemetry **3**, 99–103 (1960).

[2] Rosenbaum, R., "Longitudinal range control for a lifting vehicle entering a planetary atmosphere," ARS Paper 1911–61 (August 1961).

[3] Watson, G. N., *Theory of Bessel Functions* (Cambridge University Press, London, 1922).

[4] Jahnke, E. and Emde, F., *Tables of Functions* (Dover Publications, New York, 1945), Chap. VIII.

[5] *Bessel Functions, Part II* (Cambridge University Press, London, 1952), p. xxxv, Tables I and II.

Thrust Vector Orientation in Pilot-Controlled Lunar Landings

L. Keith Barker* and M. J. Queijo†

NASA Langley Research Center, Hampton, Va.

Nomenclature

K = angle between thrust vector and line of sight to a visual reference, deg
h = altitude above lunar surface, ft
$\dot{r}$ = radial velocity, fps
$r\dot{\theta}$ = transverse velocity, fps
R = range of travel over lunar surface, ft
ΔV = characteristic velocity, fps
F = thrust, lb
W = earth weight, lb
V = total velocity, fps

Subscripts

0 = initial condition
t = terminal condition
S = orbiting spacecraft reference

Introduction

THE primary guidance and control systems of current spacecraft are automatic. In manned space missions, however, it has been shown that man can improve the reliability of a system, if he is given the opportunity to act as a backup to the primary system. In order to permit manual control, it is necessary to provide the pilot with a suitable control system and with information pertinent to the task. In the case of the latter requirement, out-of-the-window scenes should be of great value and, in fact, might be the only information available, if the necessity for manual control is caused by a failure that affects the vehicle display panel or situation sensors.

The study to be discussed in this paper is concerned with the use of visual references for performing the lunar landing maneuver. The primary control function in this task is proper orientation of the vehicle thrust vector. The problem to be examined, therefore, is to determine if there are any convenient visual references to aid the pilot in thrust vector orientation and to determine the sensitivity of terminal conditions to errors in use of the reference or in vehicle initial conditions (start of braking maneuver).

Presented at the AIAA/NASA Third Manned Space Flight Meeting, Houston, Texas, November 4-6, 1964 (no preprint number; published in bound volume of preprints of the meeting); revision received March 22, 1964.

* Aerospace Engineer, Space Analysis Branch, Space Mechanics Division.

† Head, Space Analysis Branch, Space Mechanics Division. Member AIAA.

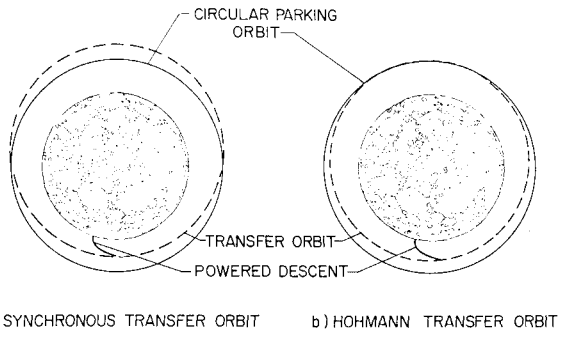

Fig. 1 Transfer orbits used in this investigation.

The procedure used in this study was to compute an efficient reference landing trajectory (gravity turn) and then to determine the orientation of the thrust vector relative to several references. The purpose was to determine if any convenient geometric relationships existed between the thrust vector and the line of sight to the various references. The references examined were the downrange and uprange horizons, the nominal landing site, and an orbiting spacecraft. All of the visual references were assumed to be in the plane of motion.

Analysis

It is assumed that a spacecraft, consisting of a command module, a service module, and a lunar excursion module, establishes a circular parking orbit 80 naut miles above the lunar surface. The lunar excursion module then separates from the spacecraft and establishes an elliptic transfer orbit having a pericynthion altitude of 50,000 ft. Two elliptic transfer orbits are being considered for the lunar mission, namely, an elliptic orbit that has the same orbital period as the circular parking orbit (Fig. 1a) and an elliptic orbit established by a 180° Hohmann transfer (Fig. 1b). At pericynthion of the transfer orbit, an efficient landing is accomplished by thrusting against the velocity vector (gravity turn).

The equations of motion used were for a point mass moving in a central force field and subject to a thrust force in the plane of motion. A constant-thrust landing engine producing an initial thrust-to-earth-weight ratio of 0.485 and having a specific impulse of 305 secs was assumed for the landing. These landing trajectories were then examined to determine the orientation of the lander thrust vector with respect to the various visual references mentioned previously.

Results and Discussion

Two types of transfer orbits were examined, one having the same period as the parking orbit (synchronous transfer) and the second being a Hohmann transfer orbit. The synchronous orbit was studied in more detail than the Hohmann, and most of this paper will be concerned with descent from the synchronous orbit.

Synchronous transfer orbit

Nominal landing trajectory: As stated in the Introduction, a gravity-turn descent was computed from the pericynthion of the synchronous orbit. The orientation of the thrust vector relative to the uprange and downrange horizons, the landing site, and the orbiting spacecraft was then examined, and the results are shown in Fig. 2. The figure shows the variation, during the landing, of the angle between the thrust vector and the line of sight to the various references. As can be seen, the angle between the thrust vector and the line of sight to the orbiting spacecraft remains very nearly constant throughout the landing maneuver. The other references do not appear to be quite as convenient.